



Supplement of

Evaluating the biological pump efficiency of the Last Glacial Maximum ocean using $\delta^{13}\text{C}$

Anne L. Morée et al.

Correspondence to: Anne L. Morée (anne.moree@uib.no)

The copyright of individual parts of the supplement might differ from the article licence.

1 Sea surface salinity restoring

We compare the ocean circulation after 1000 years of simulation in a LGM spinup with and without extra adjustments to the sea surface salinity (SSS) reference field used for salinity restoring. The adjusted spinup is the one used in our study and described in the main text. If unadjusted, the LGM SSS reference field is derived from the PI SSS reference field through the addition of a PMIP3-based sea surface salinity anomaly (Morée and Schwinger, 2019a; Morée and Schwinger, 2019b) (Fig. S1a). For the unadjusted setup NorESM-OC simulated an AMOC of 21 Sv (17 Sv for the adjusted spinup), and a Drake Passage through flow of 112 Sv (134 Sv for the adjusted spinup). The SSW profoundly decrease their volume in the Atlantic (Fig. S2). As especially the retreat of SSW is in disagreement with proxy-based reconstructions (see main text), we applied an adjustment to the SSS relaxation of -0.5 psu in the North Atlantic in the region where the anomaly was largest, as well as in the Southern Ocean (Fig. S1a). The simulated SSS for the adjusted run is shown in Fig. S1b.

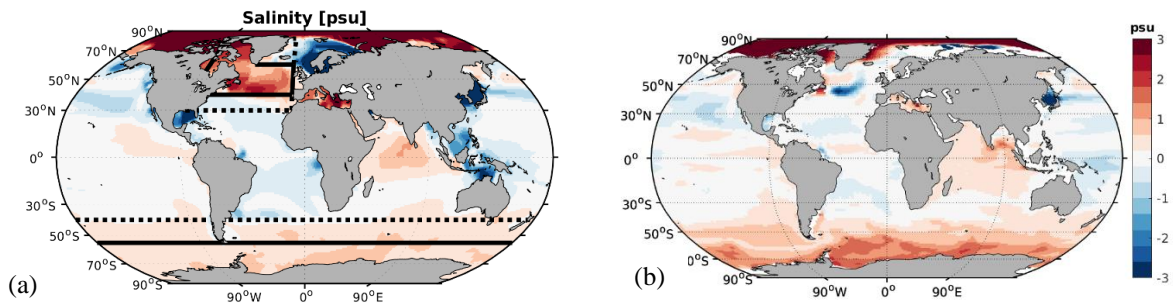


Figure S1 Sea surface salinity anomaly between the LGM and PI, with regions of salinity relaxation adjustment. (a) SSS anomaly in model forcing. In addition, the North Atlantic region, which is decreased by 0.5 psu, extends between 90°W and 45°W from 40°N to 80°N, and between 45°W to 10°W from 40°N to 60°N. The additional anomaly is linearly ramped off to zero at the line along 30°N and to the point 80°N 10°W. In the Southern Ocean, 0.5 psu is added south of 55°S, and ramped off to zero until 40°S. (b) Simulated SSS LGM-PI change.

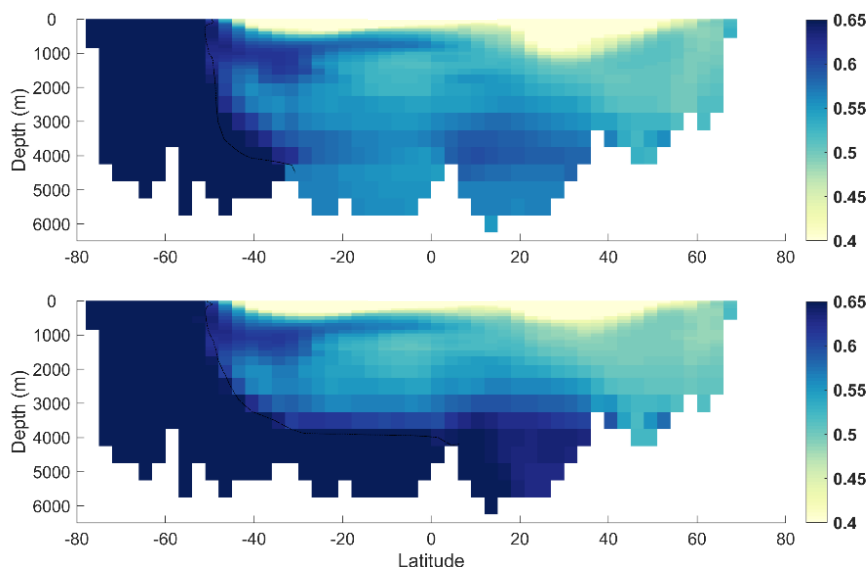


Figure S2 Atlantic PO tracer (as Fig. 1) after 1000 years of spinup without salinity adjustment (upper) and with salinity adjustment (lower).

2 LGM Normal Year Forcing

The PMIP3-based atmospheric anomaly fields which were used to obtain an atmospheric forcing representative of the LGM (Morée and Schwinger, 2019a; Morée and Schwinger, 2019b) received an update (version 2, retrievable in Morée and Schwinger, 2019a) after the model simulations for this study were finished. Version 2 is based on PMIP3 models CNRM-CM5, IPSL-CM5A-LR, GISS-E2-R, MIROC-ESM and MRI-CGCM3 for all variables including SSS. In version 1, GISS-E2-R was not included and the SSS anomaly was based on CNRM-CM5 and MIROC-ESM. We evaluated the differences in the LGM spinup after 500 model years between version 1 and version 2 of these anomaly fields. We note that the modelled circulation is not fully equilibrated yet at this stage, but limit our comparison due to computational costs. We conclude that the SSS tuning applied as described in SM1 is specific to version 1 of the forcing anomaly, and should be adjusted for version 2.

3 Bern3D model description

The Bern3D v2.0s is an Earth System model of intermediate complexity. The Bern3D model comprises a single layer energy-moisture balance atmosphere with a thermodynamic sea-ice component (Ritz et al., 2011), a seasonally forced 3-D geostrophic-frictional balance ocean (Edwards et al., 1998; Müller et al., 2006) with an isopycnal diffusion scheme and Gent-McWilliams parameterization for eddy-induced transport (Griffies, 1998), and a 10-layer ocean sediment module (Heinze et al., 1999; Tschumi et al., 2011; Jeltsch-Thömmes et al., 2019). Further, a 4-box land-biosphere model (Siegenthaler and Oeschger, 1987) is coupled to the model in order to simulate the dilution of carbon isotopic perturbations by the land biosphere. The horizontal resolution across Bern3D model components is 41×40 grid cells and 32 logarithmically spaced depth layers in the ocean. Surface wind stress is prescribed following the NCEP/NCAR monthly wind stress climatology (Kalnay et al., 1996). Carbonate chemistry, air-sea gas exchange is implemented according to OCMIP-2 protocols (Najjar and Orr, 1999; Orr et al., 1999) with updates for the ^{14}C standard ratio and half-life (Orr et al., 2017), the calculation of the Schmidt number (Wanninkhof, 2014), and the carbonate chemistry (Orr and Epitalon, 2015). In order to match observational estimates of natural and bomb-produced ^{14}C , the global mean air-sea transfer is reduced by 19% compared to OCMIP-2 (Müller et al., 2008), and the gas transfer velocity scales linearly with wind speed following Krakauer et al. (2006). The model explicitly simulates the transport by advection, diffusion, and convection of dissolved inorganic carbon and semi-labile organic carbon (DIC, DOC), the corresponding isotopic forms (DI^{13}C , DO^{13}C , DI^{14}C , DO^{14}C), as well as alkalinity (Alk), phosphate (PO_4^{3-}), oxygen (O_2), iron (Fe), silica (Si), and an ideal age tracer. Primary productivity in the ocean is a function of light availability, temperature, and phosphate and iron availability (Doney et al., 2006), and is restricted to the uppermost 75 m (Parekh et al., 2008; Tschumi et al., 2011). In the sediment, the transport, redissolution/remineralization, and bioturbation of solid material, the pore water chemistry, and diffusion are dynamically calculated in the top 10 cm (see Tschumi et al., 2011, for more details). Burial (loss) of nutrients, carbon, and alkalinity from the sediment is balanced by a variable input flux to the coastal surface ocean during spin-up. These weathering input fluxes are set equal to burial fluxes at the end of the spin-up for transient simulations. ^{13}C is implemented as a tracer across all model components and ^{13}C fluxes and inventories are explicitly simulated. Fractionation of ^{13}C is considered for atmosphere-ocean gas transfer, for carbonate chemistry, for the formation of CaCO_3 , POC, and DOC, and for photosynthesis on land. No fractionation takes place for the remineralization of organic carbon in the ocean and on land and the dissolution of

CaCO₃ in the ocean. We use the model in the same setup as described in Jeltsch-Thömmes et al. (2019). The Bern3D model components have been evaluated comprehensively in several studies (e.g., Roth et al., 2014; Battaglia et al., 2016; Jeltsch-Thömmes et al., 2019).

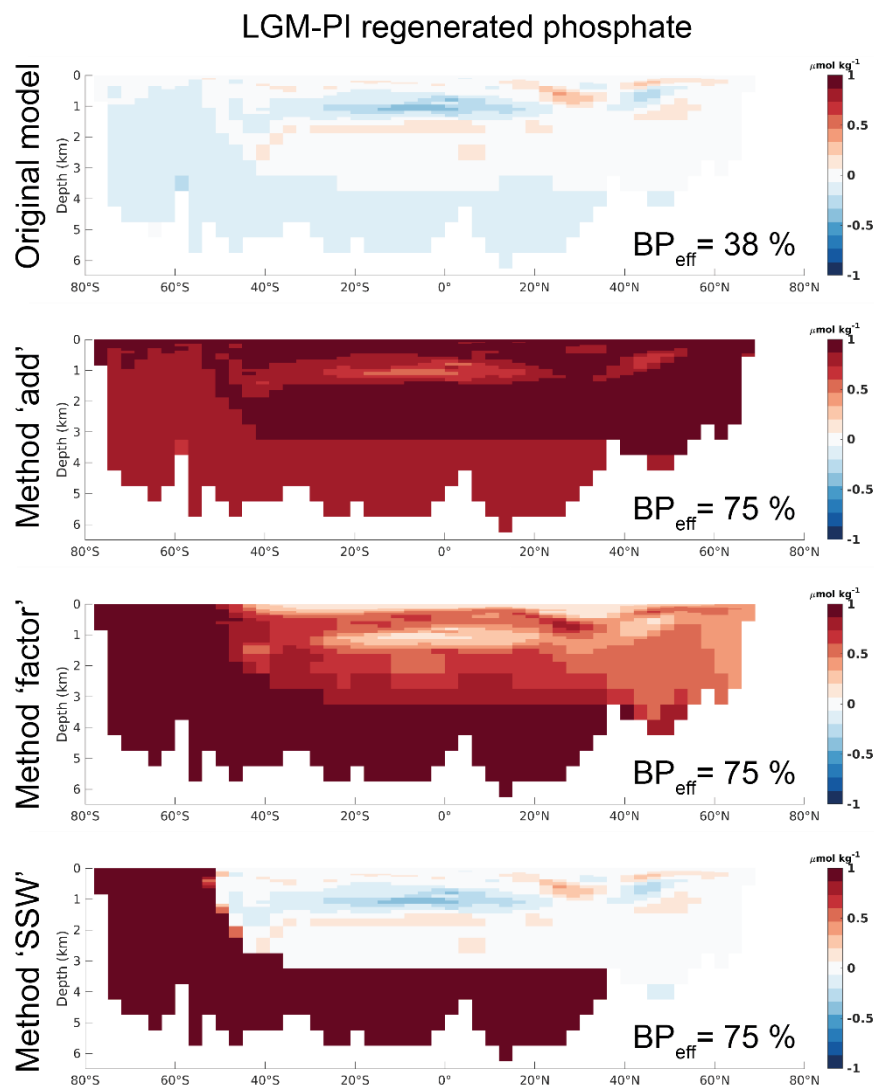


Figure S3 Atlantic transects (25-35° W) of the effect of the three different methods on the regenerated phosphate distribution for a BP_{eff} of 75%.

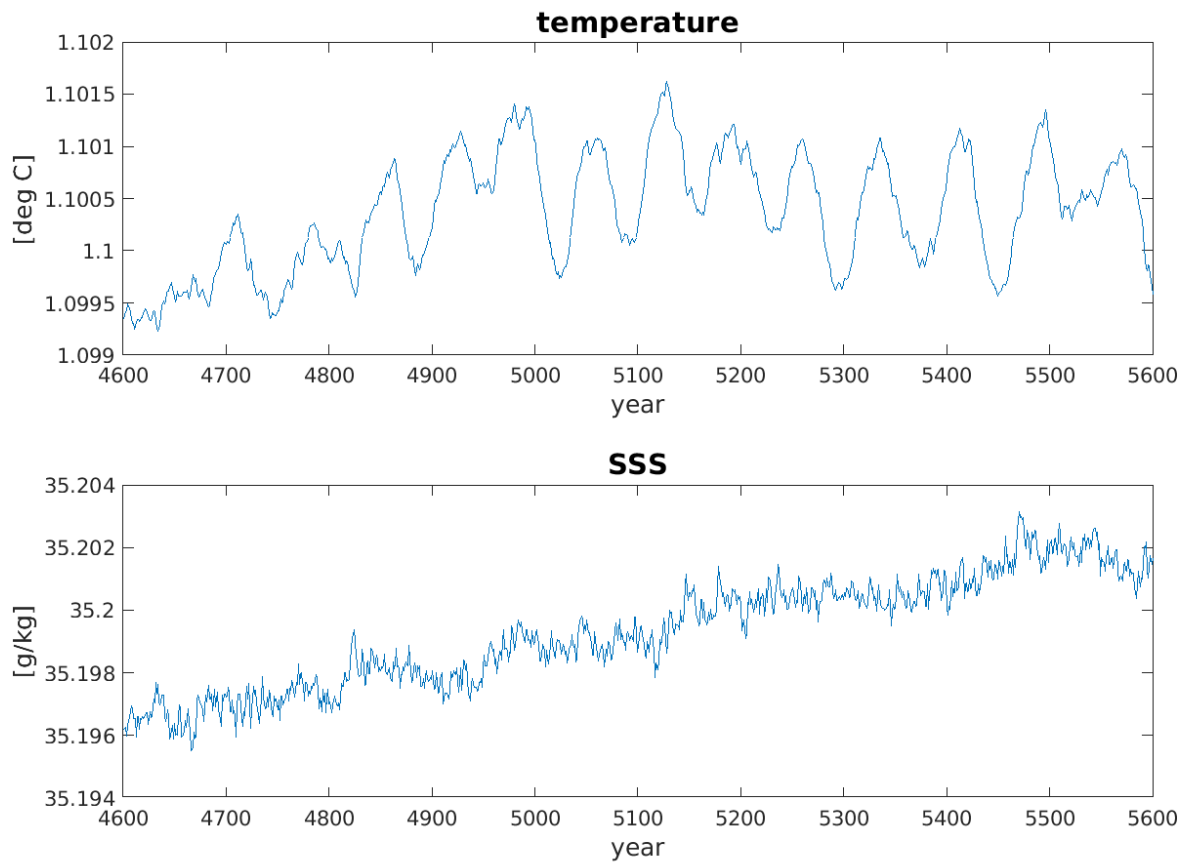


Figure S4 Average ocean temperature (top panel) and sea surface salinity (bottom panel) for the last 1000 years of the LGM simulation.

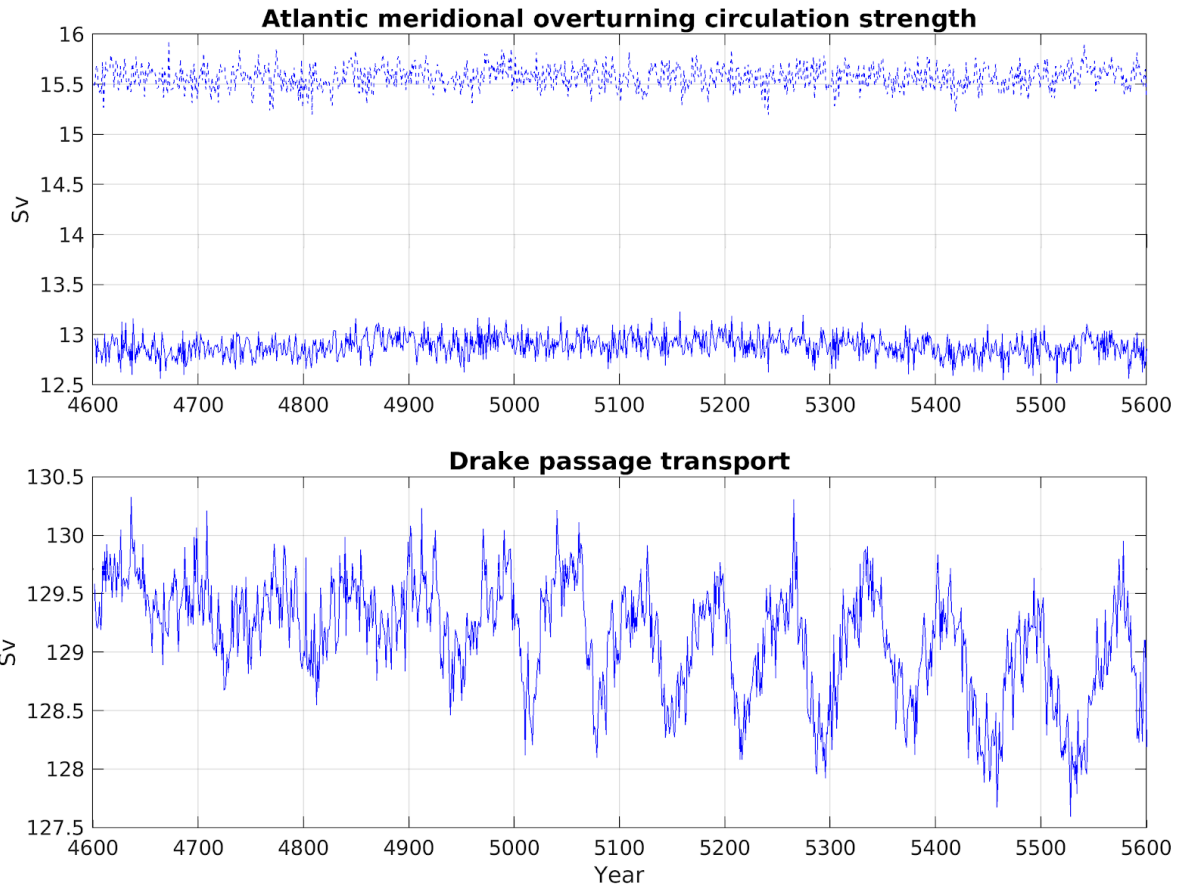


Figure S5 Strength of the Atlantic meridional overturning circulation (AMOC) at 26° N (solid line, top panel), maximum AMOC strength north of 20° N (dashed line, top panel), and sea surface salinity (bottom panel) for the last 1000 years of the LGM simulation.

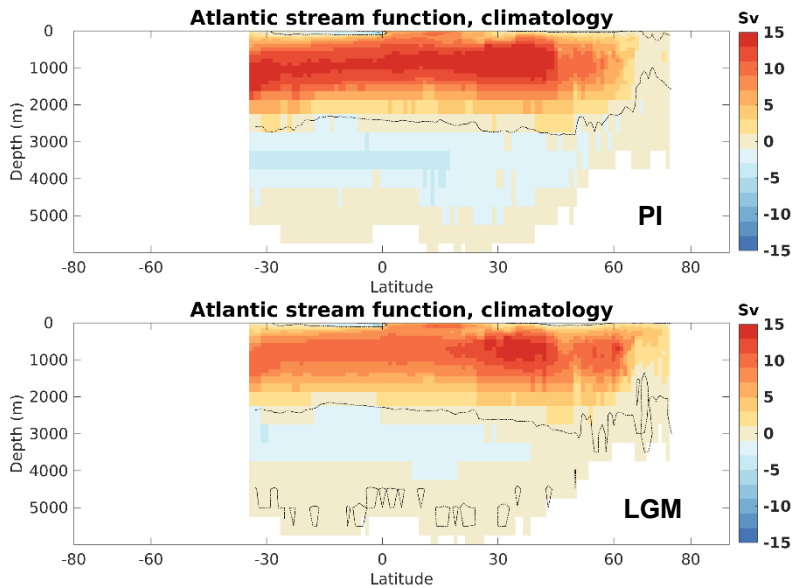


Figure S6 Atlantic stream functions (25-35° W) for the PI (top) and LGM (bottom). The depth of the transition between the Atlantic overturning cells, as indicated by the depth of the zero Sv contour at 30°S, shallowed by ~350 m in our LGM setup as compared to the PI spinup.

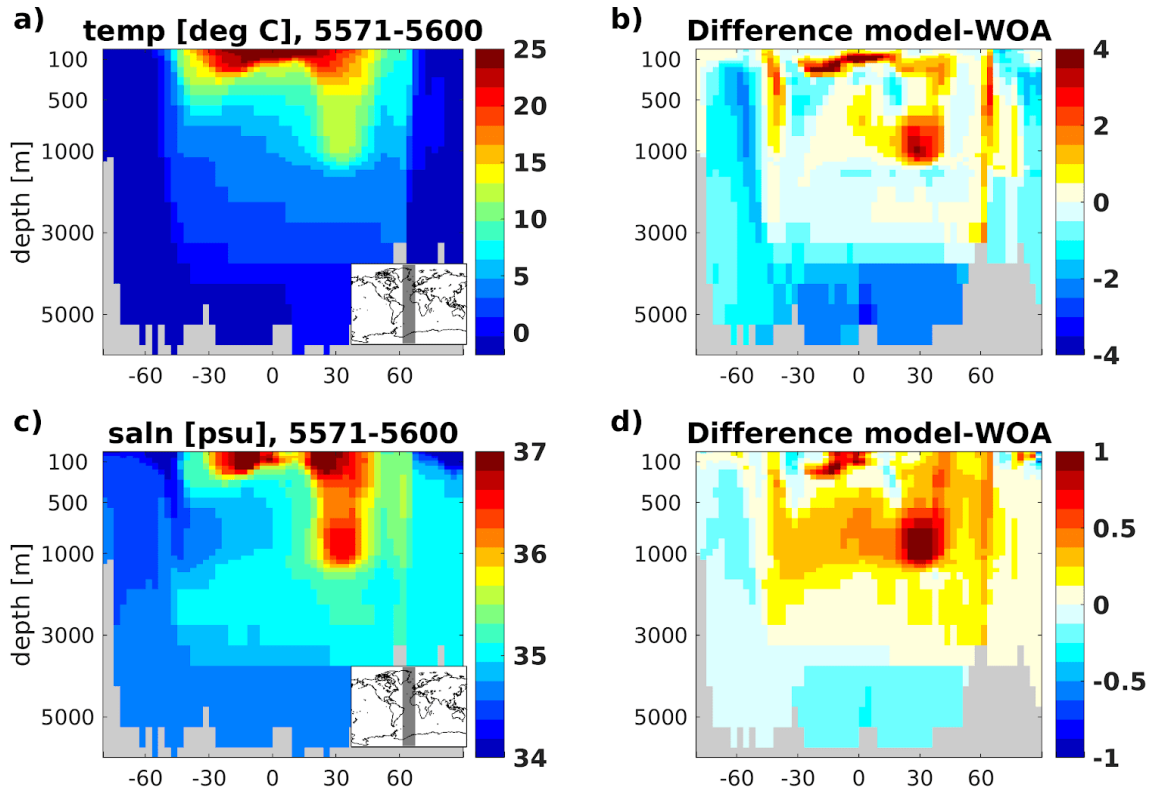


Figure S7 Zonal mean temperature (a,b) and salinity (c,d) averaged over model years 5571-5600 along the grey shaded area in the Atlantic (shown in the insets in panels a and c). Absolute values are shown in panels a and c, while the difference with the World Ocean Atlas data is shown in panels b and d.

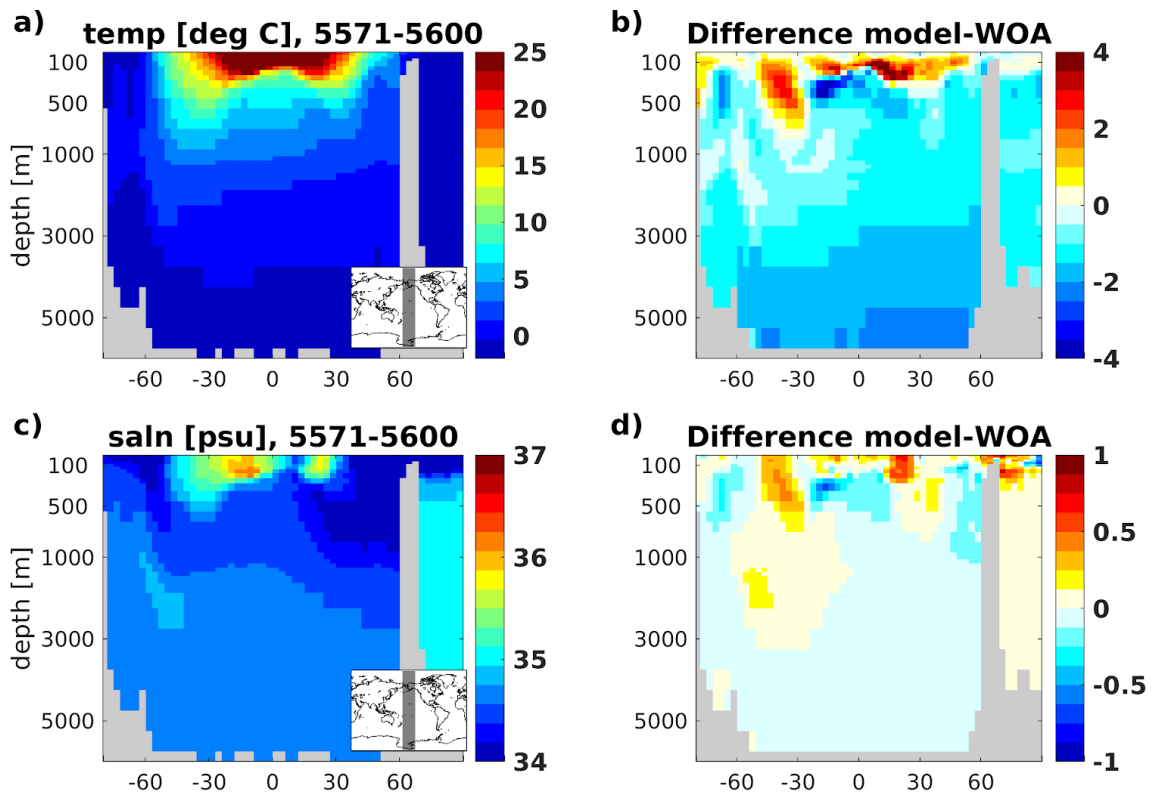


Figure S8 Same as Fig. S6, but for the Pacific Ocean.

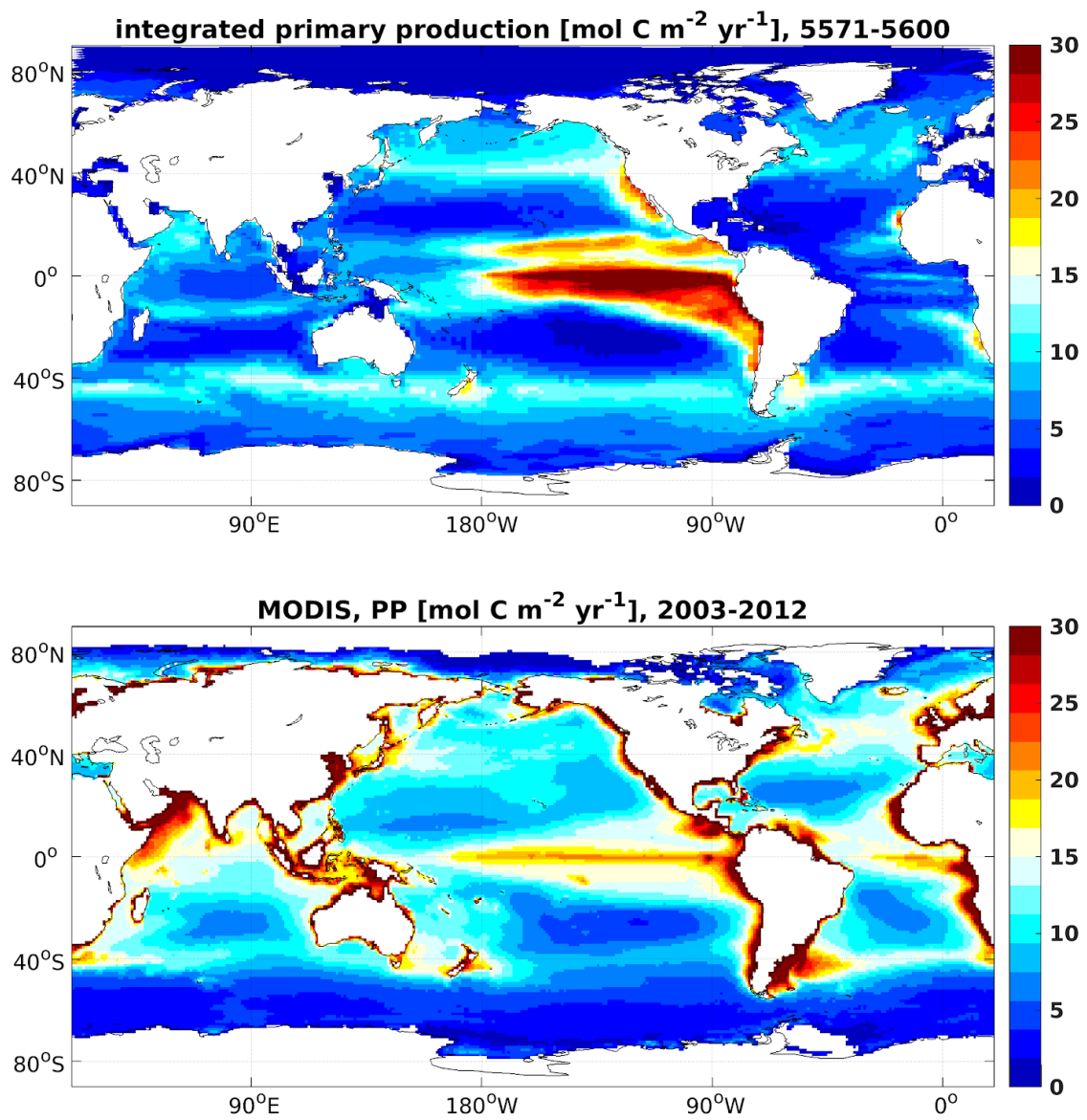


Figure S9 Primary production averaged over model years 5571-5600 (top panel), and observation based estimates of PP derived from MODIS retrievals for the years 2003 to 2012.

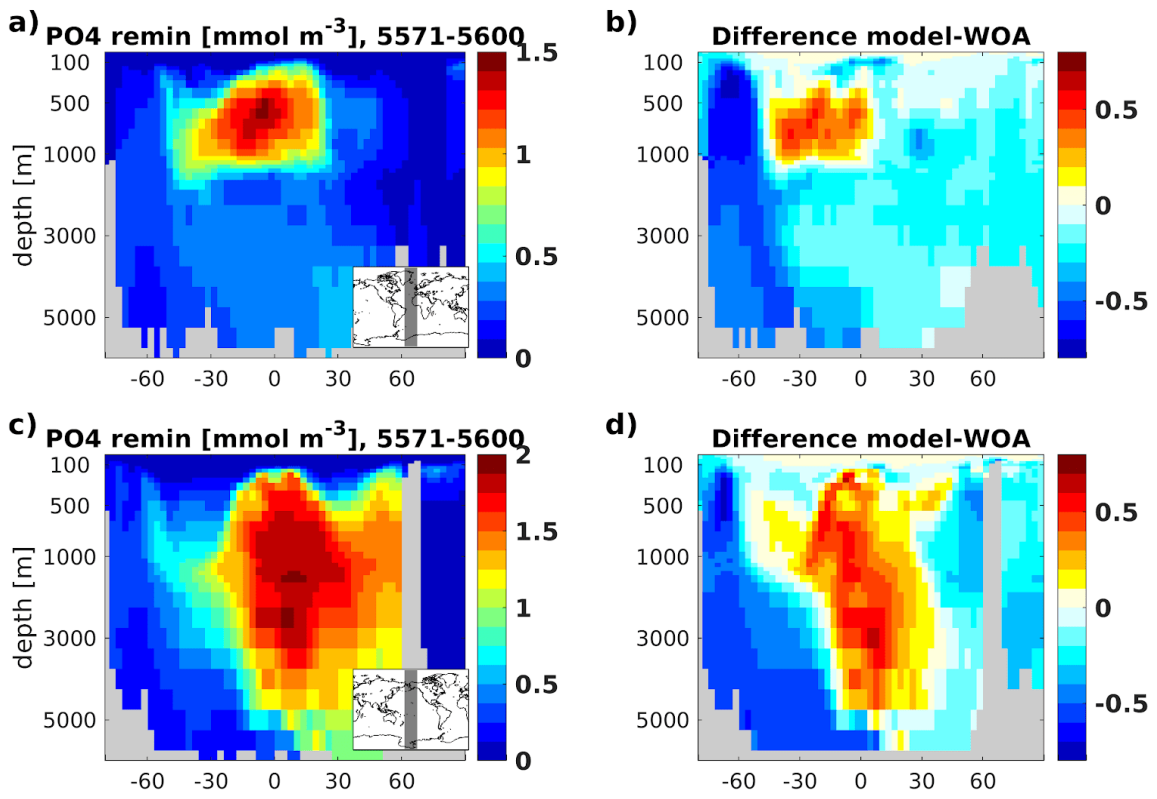


Figure S10 Zonal mean concentration of remineralized phosphate averaged over model years 5571-5600 (a,c) and the difference with respect to an estimate derived from World Ocean Atlas data (b,d) along the grey shaded areas shown in the insets in panels a and c.

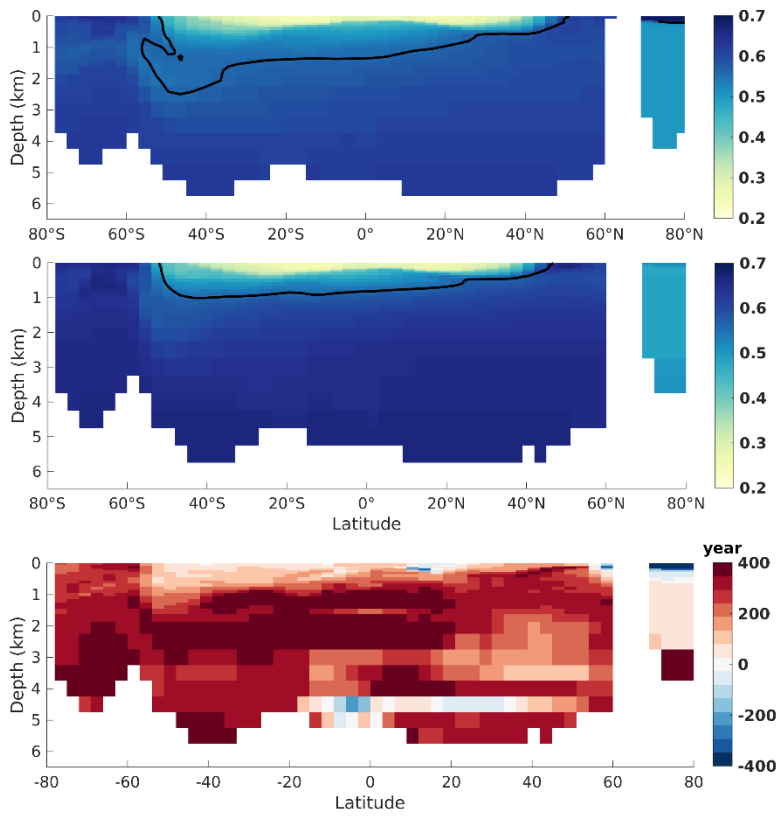


Figure S11 PO tracer Pacific zonal mean transect (175° E – 175° W) for the PI (top) and LGM (middle) simulation as well as Pacific change in radiocarbon age (bottom), as Fig. 1.

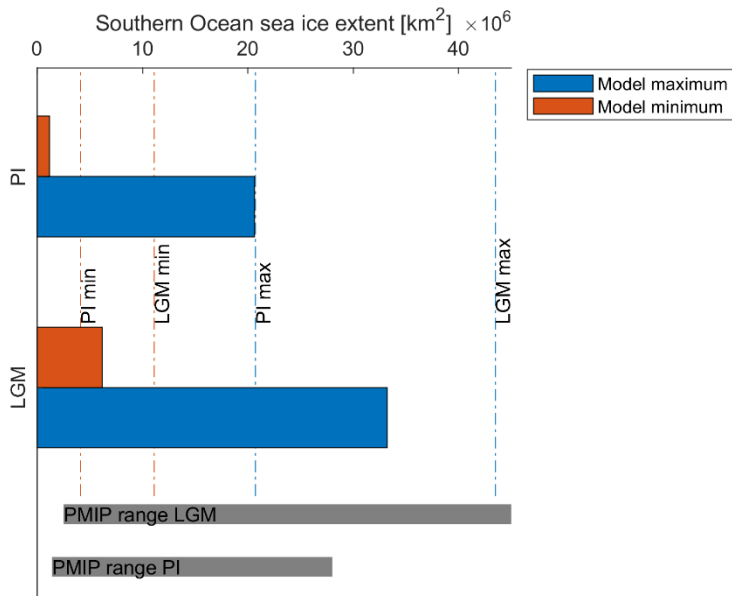


Figure S12 Southern Ocean sea ice extent (area of sea ice with a concentration of >15%) for the PI and LGM simulations. PMIP and observational estimate data from Roche et al. (2012) and Marzocchi and Jansen (2017).

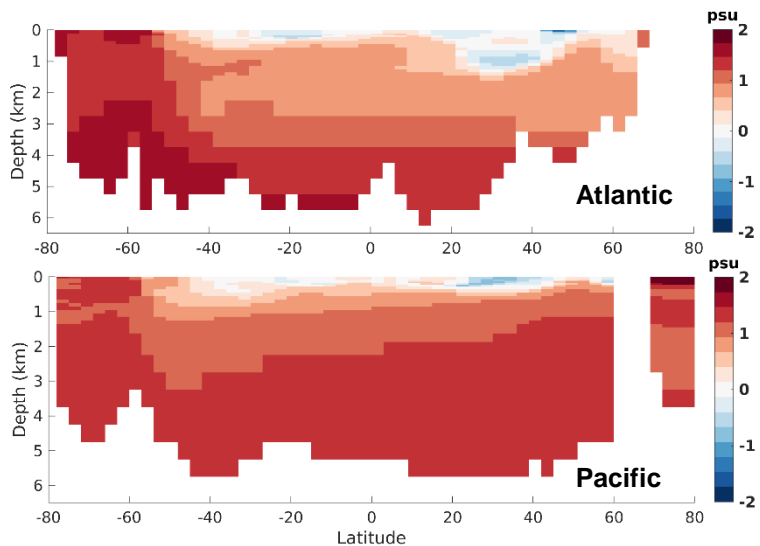


Figure S13 Simulated LGM-PI change in salinity.

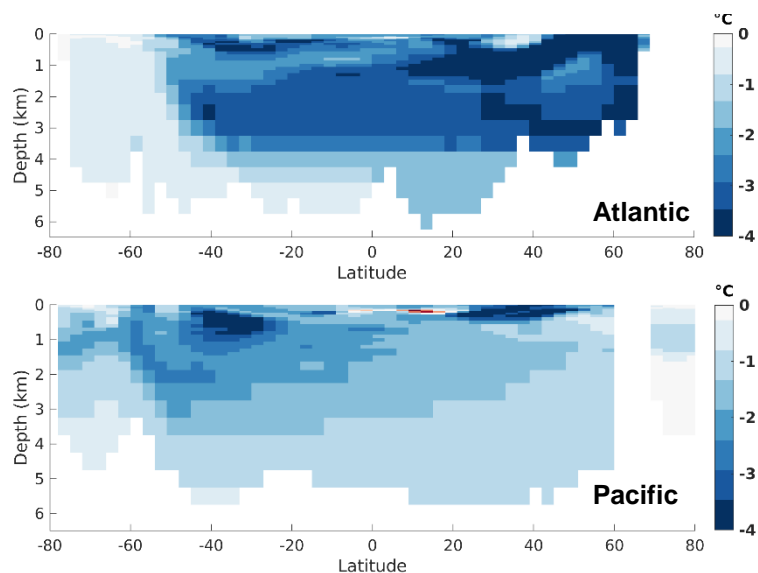


Figure S14 Simulated LGM-PI change in temperature.

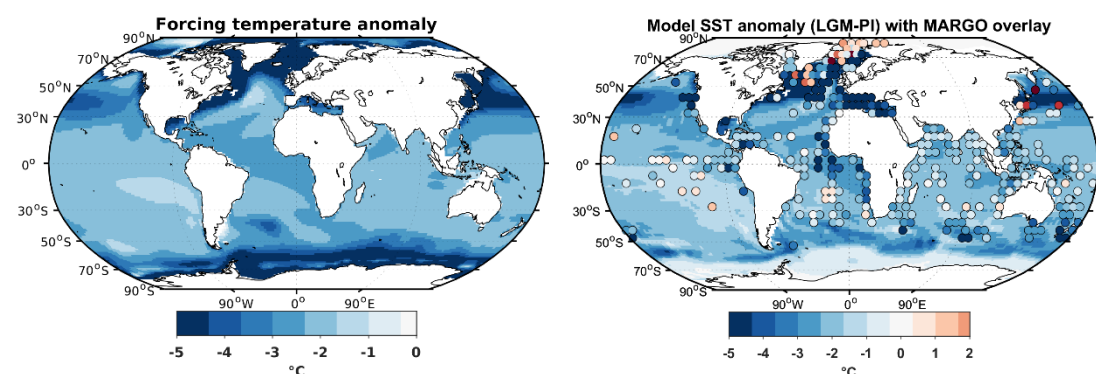


Figure S15 Atmospheric forcing (annual mean) (left) and simulated SST anomaly (right) with overlay of MARGO SST reconstruction data (Margo Project Members, 2009).

ΔDIC LGM-PI

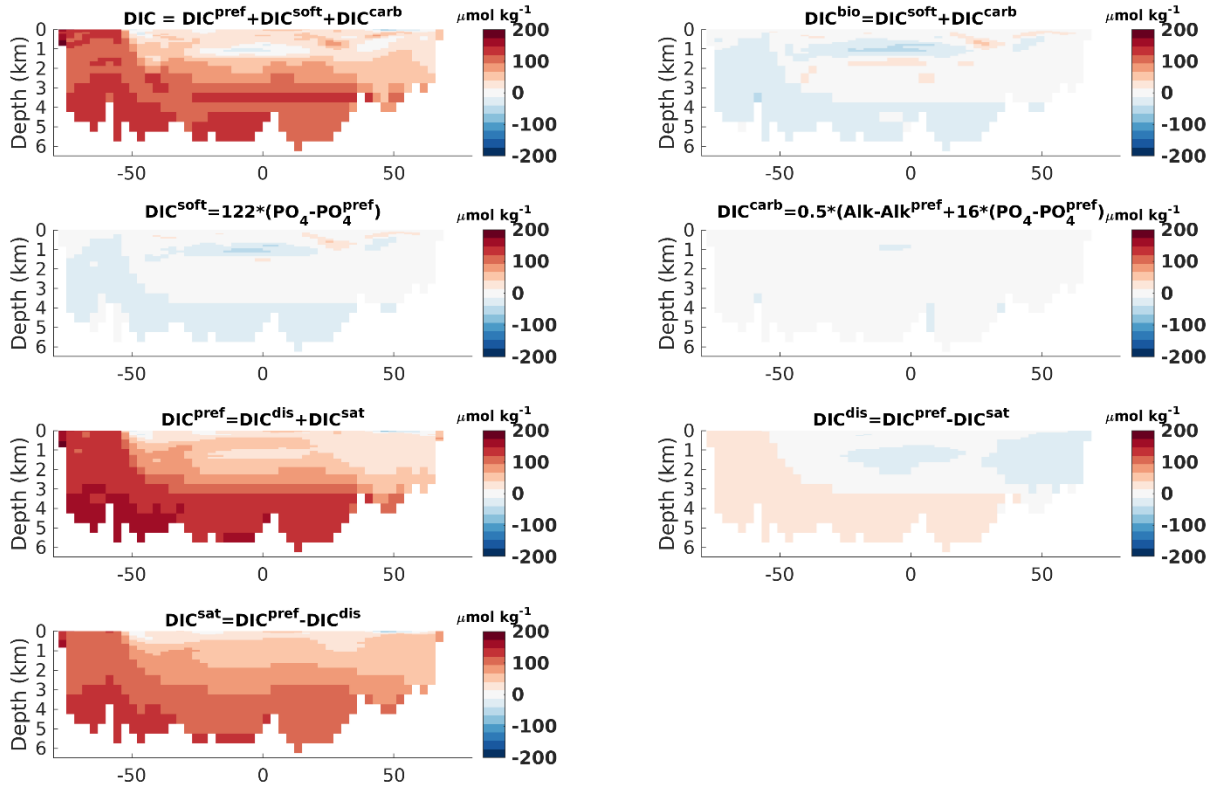


Figure S16 Atlantic zonal mean sections (25-35° W) of the different components of DIC (Bernardello et al., 2014): preformed DIC (DIC^{pref}), soft-tissue pump DIC (DIC^{soft}), DIC in equilibrium with the atmospheric $p\text{CO}_2$ at the surface of the ocean (DIC^{sat}), the DIC disequilibrium with the atmosphere (DIC^{dis}), the DIC distribution related to the formation and dissolution of CaCO_3 (DIC^{carb}) and the DIC related to all biological processes (DIC^{bio}). Preformed components are simulated as prognostic tracers in NorESM-OC (Tjiputra et al., 2020).

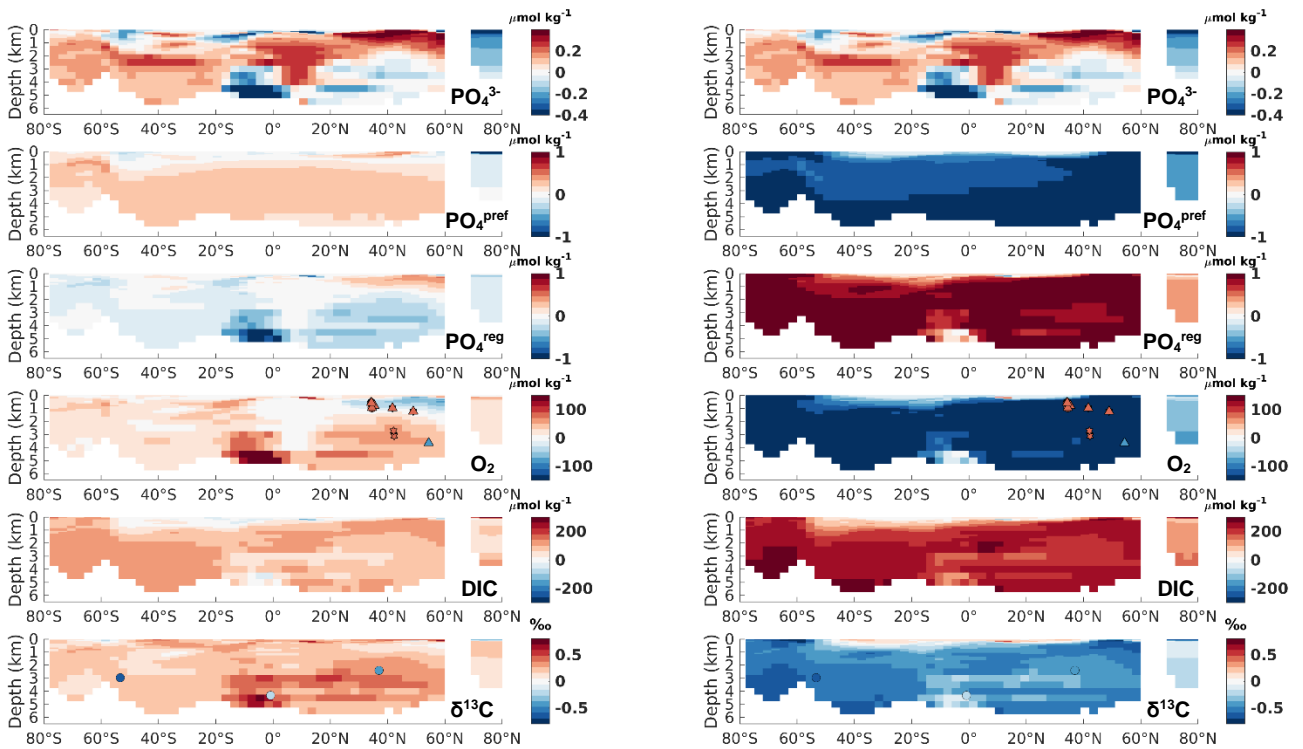


Figure S17 Pacific (175° E – 175° W) LGM-PI changes for the original model output (left-hand column) and adjusted to a biological pump efficiency of 75% (right-hand column). Otherwise as in Fig. 2 and 5.

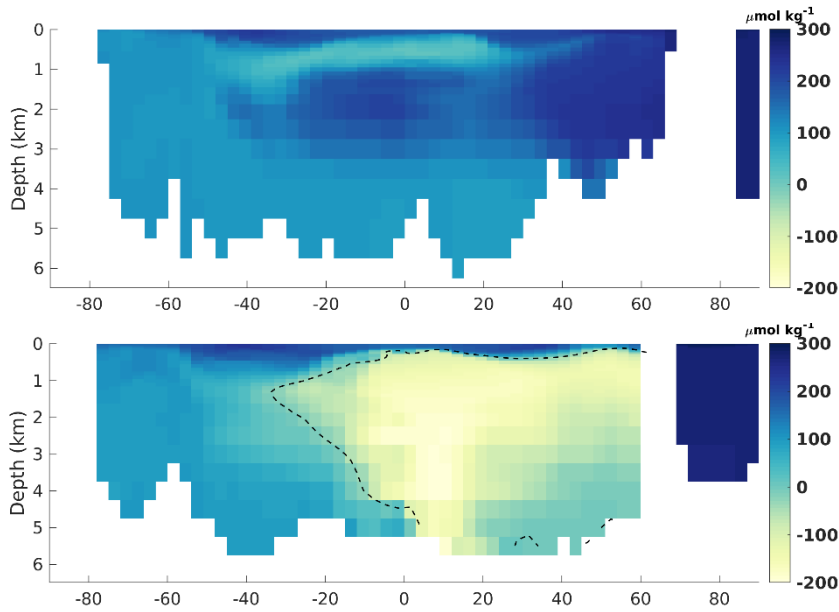


Figure S18 Simulated LGM O₂ concentrations for a 75 % \overline{BP}_{eff} , with a zero contour line.

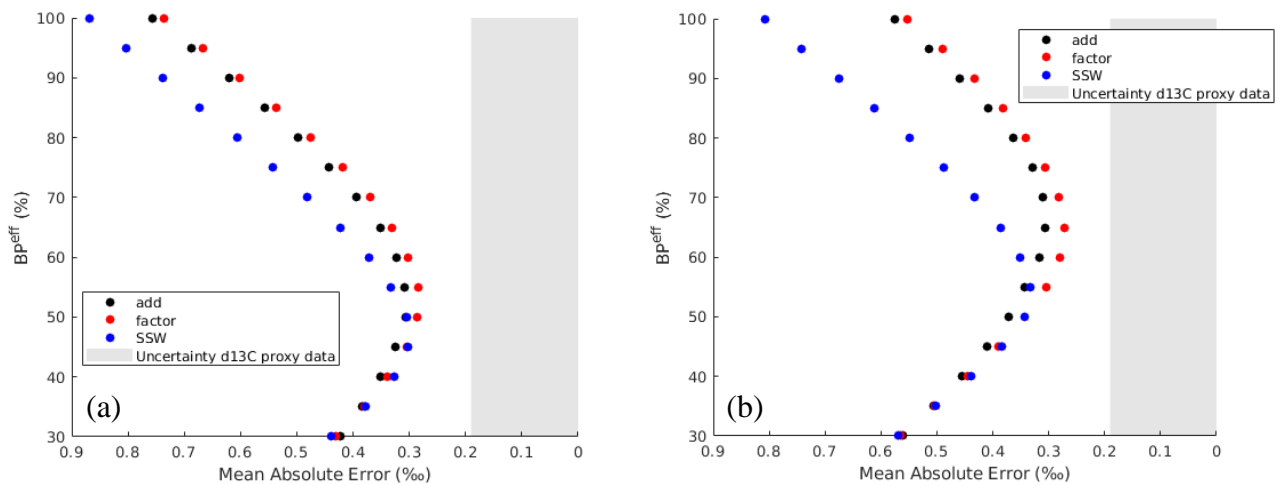


Figure S19 As in Fig. 5, but with a) simulated LGM $\delta^{13}C$ reduced by a uniform 0.4 ‰ and b) simulated LGM $\delta^{13}C$ reduced by a uniform 0.2 ‰ to account for a shift in mean marine $\delta^{13}C$.

References

- Battaglia, G., Steinacher, M., and Joos, F.: A probabilistic assessment of calcium carbonate export and dissolution in the modern ocean, *Biogeosciences*, 13, 2823-2848, 10.5194/bg-13-2823-2016, 2016.
- Bernardello, R., Marinov, I., Palter, J. B., Sarmiento, J. L., Galbraith, E. D., and Slater, R. D.: Response of the Ocean Natural Carbon Storage to Projected Twenty-First-Century Climate Change, *Journal of Climate*, 27, 2033-2053, 10.1175/JCLI-D-13-00343.1, 2014.
- Edwards, N. R., Willmott, A. J., and Killworth, P. D.: On the Role of Topography and Wind Stress on the Stability of the Thermohaline Circulation, *Journal of Physical Oceanography*, 28, 756-778, 10.1175/1520-0485(1998)028<0756:OTROTA>2.0.CO;2, 1998.
- Doney, S. C., Lindsay, K., Fung, I., and John, J.: Natural Variability in a Stable, 1000-Yr Global Coupled Climate–Carbon Cycle Simulation, *Journal of Climate*, 19, 3033-3054, 10.1175/JCLI3783.1, 2006.

Griffies, S. M.: The Gent–McWilliams Skew Flux, *Journal of Physical Oceanography*, 28, 831–841, 10.1175/1520-0485(1998)028<0831:TGMSF>2.0.CO;2, 1998.

Heinze, C., Maier-Reimer, E., Winguth, A. M. E., and Archer, D.: A global oceanic sediment model for long-term climate studies, *Global Biogeochemical Cycles*, 13, 221–250, 10.1029/98GB02812, 1999.

Jeltsch-Thömmes, A., Battaglia, G., Cartapanis, O., Jaccard, S. L., and Joos, F.: Low terrestrial carbon storage at the Last Glacial Maximum: constraints from multi-proxy data, *Climate of the Past*, 15, 849–879, 10.5194/cp-15-849-2019, 2019.

Kalnay, E., Kanamitsu, M., Kistler, R., Collins, W., Deaven, D., Gandin, L., Iredell, M., Saha, S., White, G., Woollen, J., Zhu, Y., Chelliah, M., Ebisuzaki, W., Higgins, W., Janowiak, J., Mo, K. C., Ropelewski, C., Wang, J., Leetmaa, A., Reynolds, R., Jenne, R., and Joseph, D.: The NCEP/NCAR 40-Year Reanalysis Project, *Bulletin of the American Meteorological Society*, 77, 437–472, 10.1175/1520-0477(1996)077<0437:TNYRP>2.0.CO;2, 1996.

Krakauer, N. Y., Randerson, J. T., Primeau, F. W., Gruber, N., and Menemenlis, D.: Carbon isotope evidence for the latitudinal distribution and wind speed dependence of the air–sea gas transfer velocity, *Tellus B*, 58, 390–417, <https://doi.org/10.1111/j.1600-0889.2006.00223.x>, 2006.

Marzocchi, A., and Jansen, M. F.: Connecting Antarctic sea ice to deep-ocean circulation in modern and glacial climate simulations, *Geophysical Research Letters*, 44, 6286–6295, 10.1002/2017GL073936, 2017.

Morée, A., and Schwinger, J.: Last Glacial Maximum minus pre-industrial anomaly fields for use in forced ocean modelling, based on PMIP3 [Dataset]. Norstore, 2019a.

Morée, A. L., and Schwinger, J.: A Last Glacial Maximum forcing dataset for ocean modelling, *Earth Syst. Sci. Data Discuss.*, 2019, 1–14, 10.5194/essd-2019-79, 2019b.

Müller, S. A., Joos, F., Edwards, N. R., and Stocker, T. F.: Water Mass Distribution and Ventilation Time Scales in a Cost-Efficient, Three-Dimensional Ocean Model, *Journal of Climate*, 19, 5479–5499, 10.1175/JCLI3911.1, 2006.

Müller, S. A., Joos, F., Plattner, G. K., Edwards, N. R., and Stocker, T. F.: Modeled natural and excess radiocarbon: Sensitivities to the gas exchange formulation and ocean transport strength, *Global Biogeochemical Cycles*, 22, <https://doi.org/10.1029/2007GB003065>, 2008.

Najjar, R. G., and Orr, J. C.: Biotic-HOWTO. Internal OCMIP, Tech. rep., LSCE/CEA, Saclay, Gif-sur-Yvette, France, 1999.

Orr, J. C., Najjar, R., Sabine, C. L., and Joos, F.: Abiotic-HOWTO. Internal OCMIP, Tech. rep., LSCE/CEA, Saclay, Gif-sur-Yvette, France, 1999.

Orr, J. C., and Epitalon, J. M.: Improved routines to model the ocean carbonate system: mocsy 2.0, *Geosci. Model Dev.*, 8, 485–499, 10.5194/gmd-8-485-2015, 2015.

Orr, J. C., Najjar, R. G., Aumont, O., Bopp, L., Bullister, J. L., Danabasoglu, G., Doney, S. C., Dunne, J. P., Dutay, J. C., Graven, H., Griffies, S. M., John, J. G., Joos, F., Levin, I., Lindsay, K., Matear, R. J., McKinley, G. A., Mouchet, A., Oschlies, A., Romanou, A., Schlitzer, R., Tagliabue, A., Tanhua, T., and Yool, A.: Biogeochemical protocols and diagnostics for the CMIP6 Ocean Model Intercomparison Project (OMIP), *Geosci. Model Dev.*, 10, 2169–2199, 10.5194/gmd-10-2169-2017, 2017.

Parekh, P., Joos, F., and Müller, S. A.: A modeling assessment of the interplay between aeolian iron fluxes and iron-binding ligands in controlling carbon dioxide fluctuations during Antarctic warm events, *Paleoceanography*, 23, <https://doi.org/10.1029/2007PA001531>, 2008.

Ritz, S. P., Stocker, T. F., and Joos, F.: A Coupled Dynamical Ocean–Energy Balance Atmosphere Model for Paleoclimate Studies, *Journal of Climate*, 24, 349-375, 2011.

Roche, D. M., Crosta, X., and Renssen, H.: Evaluating Southern Ocean sea-ice for the Last Glacial Maximum and pre-industrial climates: PMIP-2 models and data evidence, *Quaternary Science Reviews*, 56, 99-106, <https://doi.org/10.1016/j.quascirev.2012.09.020>, 2012.

Roth, R., Ritz, S. P., and Joos, F.: Burial-nutrient feedbacks amplify the sensitivity of atmospheric carbon dioxide to changes in organic matter remineralisation, *Earth Syst Dynam*, 5, 321-343, [10.5194/esd-5-321-2014](https://doi.org/10.5194/esd-5-321-2014), 2014.

Siegenthaler, U., and Oeschger, H.: Biospheric CO₂ emissions during the past 200 years reconstructed by deconvolution of ice core data, *Tellus B*, 39B, 140-154, <https://doi.org/10.1111/j.1600-0889.1987.tb00278.x>, 1987.

Tjiputra, J. F., Schwinger, J., Bentsen, M., Morée, A. L., Gao, S., Bethke, I., Heinze, C., Goris, N., Gupta, A., He, Y. C., Olivie, D., Seland, Ø., and Schulz, M.: Ocean biogeochemistry in the Norwegian Earth System Model version 2 (NorESM2), *Geosci. Model Dev.*, 13, 2393-2431, [10.5194/gmd-13-2393-2020](https://doi.org/10.5194/gmd-13-2393-2020), 2020.

Tschumi, T., Joos, F., Gehlen, M., and Heinze, C.: Deep ocean ventilation, carbon isotopes, marine sedimentation and the deglacial CO₂ rise, *Clim. Past*, 7, 771-800, [10.5194/cp-7-771-2011](https://doi.org/10.5194/cp-7-771-2011), 2011.

Wanninkhof, R.: Relationship between wind speed and gas exchange over the ocean revisited, *Limnology and Oceanography: Methods*, 12, 351-362, [10.4319/lom.2014.12.351](https://doi.org/10.4319/lom.2014.12.351), 2014.